Nanoscale Resolution 3D Snapshot Particle Tracking by Multifocal Microscopy

Xiaolei Wang[1], Hannah Yi[2], Itay Gdor[1], Mark Hereld[3], and Norbert F. Scherer[1,2,4,*]

[1]James Franck Institute, University of Chicago, 929 E. 57th St., Chicago, IL 60637, USA

[2] Department of Chemistry, University of Chicago, 5801 S. Ellis Ave., Chicago, IL 60637, USA

[3] Mathematics and Computer Science Division, Argonne National Laboratory, 9700 S. Cass Avenue, Lemont, IL USA

[4] Institute for Biophysical Dynamics, University of Chicago, 929 E. 57th St., Chicago, IL 60637, USA

*nfschere@uchicago.edu

1. Diffractive optical element fabrication and characterization

The DOE for multifocal microscopy (MFM) was designed to create a 3x3 array of sub-images (tiles) that have a focal shift of 600 nm.[1,2] The binary patterned DOE fabricated for the present study has a unit cell period of 56 μm and design focal shift, Δz, of 600nm. Our DOE is designed for a (fluorescence) wavelength of 610nm with emission light distributed evenly and efficiently (67%) among the nine tiles. We fabricated the DOE in-house on a 5 mm thick 25mm diameter UV fused silica substrate (WG41050, Thorlabs). The fused silica window was cleaned with acetone, isopropyl alcohol and distilled water, then spin-coated with a 1.5μm thick layer of AZ1512 photoresist (Shipley). A laser writer (Heidelberg MLA150) exposed the desired pattern at 0.5μm pixel resolution in the photoresist (405 nm laser at a dose of 150 mJ/cm^2). The photoresist was developed in AZ-300 MIF developer (Integrated Micro Materials) for 20 s. The window

with the pattern written in photoresist was etched in a reactive ion etcher (RIE, Oxford Instruments). The glass substrate was etched to a depth of 680nm for the design wavelength of 610nm using Ar gas (25 standard cubic centimeters per minute (sccm)) and CHF_3 (25 sccm), and 200 W RF power for about 28 min. The photoresist remaining after etching was stripped with acetone in an ultrasonic bath. The etching depth and surface roughness of the DOE were measured with contact profilometry (Bruker Dektak XT-S profilometer). All fabrication steps were completed at the Pritzker Nanofabrication Facility and the Searle Cleanroom Facility at the University of Chicago.

The DOE lateral imaging and axial focal properties were characterized by imaging 200nm diameter fluorescence beads (ThermoFisher, F8810) immobilized on a cover glass; the bead sample was scanned along the z-axis in 50nm steps using a closed-loop piezo translator (MadCity, Nano-Z200). The beads were successively focused in each consecutive tile of the MFM image in this z stack (see video 3 in the Supporting Information). Figure S1a and Figure S1b show the bead focused at tile #2 and #8 at two different z positions of the bead-on-coverslip sample. The particular chromatic aberrations present in each tile were removed by deconvolution with the corresponding 3D point spread functions (PSFs) of each tile using Huygens (Scientific Volume Imaging, Hilversum, The Netherlands). We used two image processing methods to determine the focal shift: (i) 1D Gaussian fitting for the z position of a fluorescent bead; and (ii) 3D localization using Imaris software (Oxford Instruments). Figure S1c shows the normalized fluorescence intensity distributions of the bead that appear successively in-focus in each of the nine tiles, which were fitted to Gaussian curves in z. The positions of best focus for each tile are shown in Figure S1d as red crosses and green dots, respectively, for these two methods. It is clear that there is negligible difference between the results using these two methods, which demonstrates the accuracy of focal shift determination of our image processing method. The slope of the linear fitted line establishes the focal shift, Δz, to be 650nm. This focal shift is slightly larger than what we designed for (i.e., 600nm) because the equation used for the design is a first order approximation of the transverse phase description (function) of a lens[1].

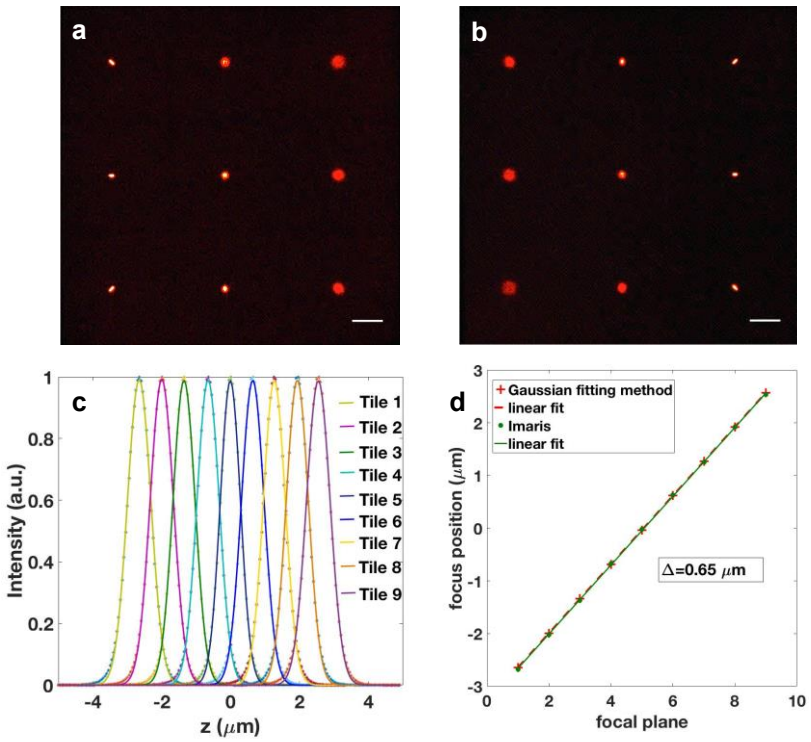

Figure S1. Characterization of the diffractive optical element (DOE). (a) and (b) are MFM images of a single fluorescent bead at two different z positions. These raw MFM images show the bead focused at tile 2 (a) and 8 (b), respectively. Scale bar (white) is 10 μm with a 33x33μm^2 field of view. (c) Gaussian curves fitted to the fluorescence signal of a 200nm diameter bead that was scanned along the z-axis with a closed-loop piezo translation stage (MadCity, Nano-Z200). Each curve is the signal from each individual tile for the sequence of z positions of the stage and sample. (d) Plot of the focus position of each tile obtained from the fitted centroids of the focal shift curves from Fig. (c) (red crosses) and Imaris (green dots). The linear fit has a slope of Δz=650nm/tile or per focal plane, which is the experimentally determined focal shift between tiles. The goodness of fit substantiates that the focal shift is constant for the 9 tiles (planes) of the MFM DOE. Note the magnitude of the focal shift is slightly larger than the design target due to the first order lens approximation used in the design.

2. MFM image reconstruction

Reconstructing a 3D image from the set of nine 2D multifocal images involves a series of steps: (i) arranging the nine focal plane images in order of the focal shift; (ii) aligning them laterally using a flood image; (iii) deconvolving each image with the corresponding measured point spread function using Huygens; (iv) aligning them into a 3D stack with a transformation matrix approach that was calibrated using a set of 200 nm fluorescent beads (ThermoFisher, F8810) immobilized on a coverslip; and (v) interpolating

the 3D stack of 9 planes into a 3D stack with 81 planes. We term this procedure multi-tile deconvolution shift-error correction and interpolation (MTD-SEC-I). A flood image was obtained with a fluorescent plastic slide (Chroma) with an excitation wavelength of 575nm and the same emission filters as for the mCherry fluorescent protein imaging. This measurement allows determining the borders of the 9 tiles using a threshold of the flood image.

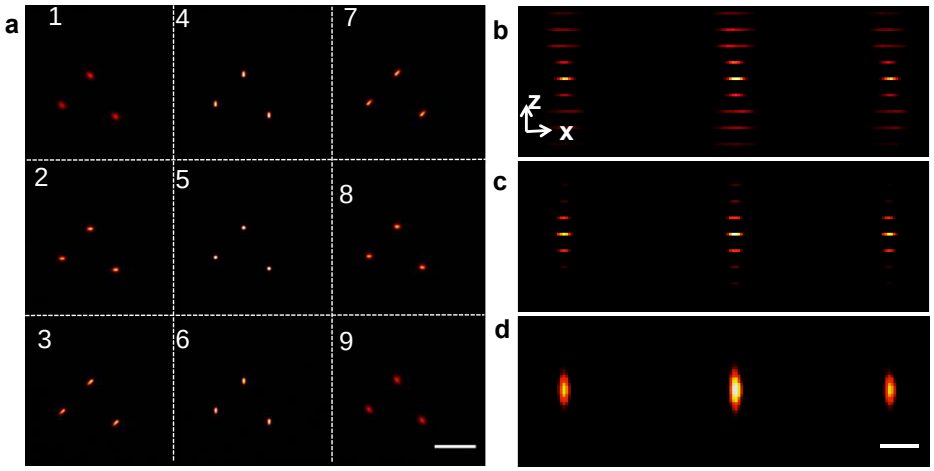

Figure S2. Details of image processing to create a 3D MFM image. (a) A single frame (image) of MFM data (9 tiles or focal planes) of three 200nm fluorescent beads viewed in the xy plane perspective. Scale bar is 10 μm. (b) The xz projection of the raw data. (c) The xz projection of the MFM data processed by deconvolution and shift error correction. (d) The xz projection of the MFM data processed with multi-tile deconvolution and shift error correction and interpolation (MTD-SRC-I). Scale bar is 2 μm.

Figure S2 is an MFM image of three 200nm diameter fluorescent beads obtained using 610nm LED illumination and the same filters as for mCherry imaging (see below). Figure S2b shows side-on planarized projections of the 9 focal plane-shifted images following coarse alignment based on the flood image. It is clear that there is an x, y shift between different focal planes and significant achromatic aberration. The point spread function (PSF) that removes the achromatic aberration with deconvolution was obtained with 100nm fluorescent beads (ThermoFisher, F8801). A z-stack of MFM images is measured by scanning the bead sample along the z-axis in 50nm steps using a closed-loop piezo translator. In this z stack, the beads successively come into focus in each MFM image tile. Nine 3D PSFs, one for each tile, were obtained with PSF distiller in Huygens. Chromatic aberration and the out-of-focus background were removed for each

focal plane (i.e., for each different tile) by deconvolution with the appropriate (one of nine) 3D PSFs using Huygens. The positions of maximum intensity of the three 200nm fluorescent beads in each tile (different focal planes) were used to determine the transformation matrix for fine alignment; i.e., by translation, rotation and scaling.[3] Finally, the nine deconvoluted focal planes were accurately superimposed using the transformation matrix as shown in Fig. S2c. New data points are constructed by interpolation between the nine focal planes resulting in continuous looking 3D images of the fluorescent beads (Fig. S2d).

The elimination of chromatic aberration by PSF deconvolution of each individual tile, as opposed to using a second diffractive optical element and multifaceted prism for this purpose, is discussed in detail elsewhere.[4]

3. Validation of MFM 3D image reconstruction

To validate MFM 3D image reconstruction by the MTD-SEC-I approach, we use a 3D confocal z-stack image as "ground truth". The FARMER method[3] allows us to successfully correlate images across the confocal microscopy and MFM platforms. We calculated the standard deviation for position differences of identical sets of fluorescent beads imaged by confocal microscopy and MFM. Confocal microscopy was performed using a Yokogawa W1 spinning disk confocal with a 100x oil immersion objective (Nikon 100x NA 1.45, MRD01905) with an EMCCD array detector (Andor iXon Ultra 888). The objective was moved in 50 nm steps to obtain confocal z stacks.

Figure S3a shows a 3D deconvolved confocal image of 200nm diameter fluorescent beads (ThermoFisher, F8810) embedded in 2% agarose gel. Figure S3b is the xz projection of the confocal data. Figure S3c shows the reconstructed MFM image with 3D deconvolution using a single 3D PSF generated from one MFM frame (the center tile is in focus). Comparing the bead axial positions to the positions of the identical beads imaged and localized from confocal z-stacks gives a large standard deviation of 70nm in axial particle localization (for the 3D deconvolved MFM data). This large error of localization is paralleled by a significant distortion of the shape of the beads located near the axial limits of the 3D deconvolved MFM image volume. This result demonstrates that 3D deconvolution with a single 3D PSF

does not work for MFM reconstruction since shift invariance is not satisfied by the 3D PSF because of different chromatic aberration in each MFM tile.

By contrast, Figure S3d shows that the MFM image is accurately reconstructed in 3D with the MTD-SEC-I approach described in detail in our discussion of Figure S2. The axial localization (error) using the multi-tile deconvolution and interpolation approach is 17nm standard deviation, which is determined by again comparing with the confocal microscopy "ground truth" localization data.

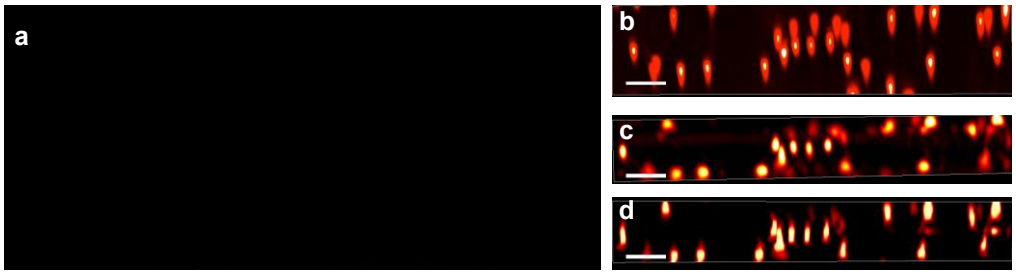

Figure S3. Correlated images between identical regions of the same bead-in-gel sample measured by confocal microscopy (ground truth) and MFM. (a) A 3D confocal image of 200nm fluorescent beads in an agarose gel. Scale bar is 3 μm. (b) is the xz projection of the confocal data. (c) The xz projection of the MFM data processed with 3D deconvolution with a single PSF and interpolation. (d) The xz projection of the MFM data processed with the nine multi-tile PSF deconvolution and interpolation (MTD-SEC-I) approach.

4. Fabrication and characterization of a DOE with 400nm focal shift.

We fabricated and characterized a second DOE for multifocal microscopy (MFM) to further confirm the process described above and to give consideration to possible trade-offs of localization error vs. extent of axial range that is useful for 3D localization and tracking. The details of design and fabrication are the same as described above; the second DOE was designed to create a 3x3 array of sub-images (tiles) that have a focal shift of 400 nm[1,2] and for a (fluorescence) wavelength of 610nm. With careful alignment, the emission light was distributed evenly and efficiently (67%) among the nine tiles. All fabrication steps were as described above and completed at the Pritzker Nanofabrication Facility and the Searle Cleanroom Facility at the University of Chicago.

The DOE lateral imaging and axial focal properties were characterized by imaging 100nm diameter fluorescence beads (ThermoFisher, F8810) immobilized on a cover glass by scanning the bead sample along

the z-axis in 100nm steps using the same closed-loop piezo translator (MadCity, Nano-Z200) in the same solution used for studies of diffusing bead samples (i.e., 50% glycerol:water). A single bead used for PSF determination was successively focused in each consecutive tile of the MFM image in this z stack (see video 4 in the Supporting Information; imaging parameters; 100nm focal shift, 0.5 Hz frame rate, 100x gain on the EMCCD detector). Figure S4a and Figure S4b show the MFM image defocused slightly above the bead (i.e. focused in the solution; the bead is below the focal plane) and the bead in focus at the center tile. The particular chromatic aberrations present in each tile were removed by deconvolution with the corresponding 3D point spread functions (PSFs) of each tile using Huygens (Scientific Volume Imaging, Hilversum, The Netherlands).

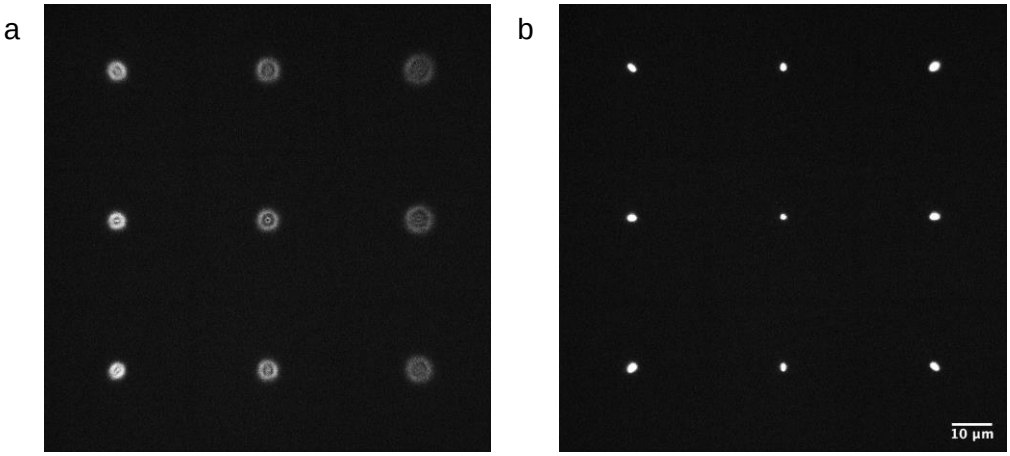

Figure S4. Point spread function measured using a 100nm diameter red (610nm emission) fluorescent bead. Snapshots taken from axial positions (a) out-of-focus and (b) in-focus at the center tile. The tile ordering starts at the bottom left tile (up the column) to the top right tile. This order represents the focal plane closest to the coverslip to the focal place furthest from the coverslip that forms the bottom of the sample cell and the inverted optical microscope.

Similar to the analysis for Figure S1, we used 1D Gaussian fitting to determine the z position of fluorescent beads (200nm dia.) in each tile. We measured three 200nm diameter fluorescent beads, shown in Figure S5a. This measurement is also used to shift-correct and construct the 3D MFM image of the three beads, in Figure S5b, which is explained in further detail below. Figure S5c shows the normalized fluorescence intensity distributions of a single bead that appears successively in focus in each of the nine tiles, which were fitted to Gaussian curves in z. The positions of best focus for each tile are shown as blue

dots (for 3 beads/measurements) in Figure S5d, while the tile-to-tile focal shifts are shown as red crosses. The slope of the fitted line establishes the focal shift, Δz, to be 418 +/- 5.7nm. This focal shift is slightly larger than what we designed for (i.e., 400nm) because the equation used for the design is a first order approximation of the transverse phase description (function) of a lens.[1] The tile-to-tile focal shifts are very consistent. However, this consistency is strongly dependent on the alignment of the DOE in the 4f relay system shown in Figure 1.

The alignment of the 9 tiles was performed as described above on the image data shown in Figure S5a and also in video 5. Three 200nm dia. beads were immobilized to a coverslip and were scanned in the axial direction (200msec exposure time, 5 frames per second, 100nm/step, 300 steps total). The video data of the 3 beads show a strikingly clear view of the axial interference associated with the axial Airy function and the delay that occurs as a result of the different focal planes in each tile (see center pixels of each bead image).[5] We obtained the 3D deconvoluted images shown in Figure 5b using Imaris applying the MTD-SEC-I approach described above (see text near Figure S2).

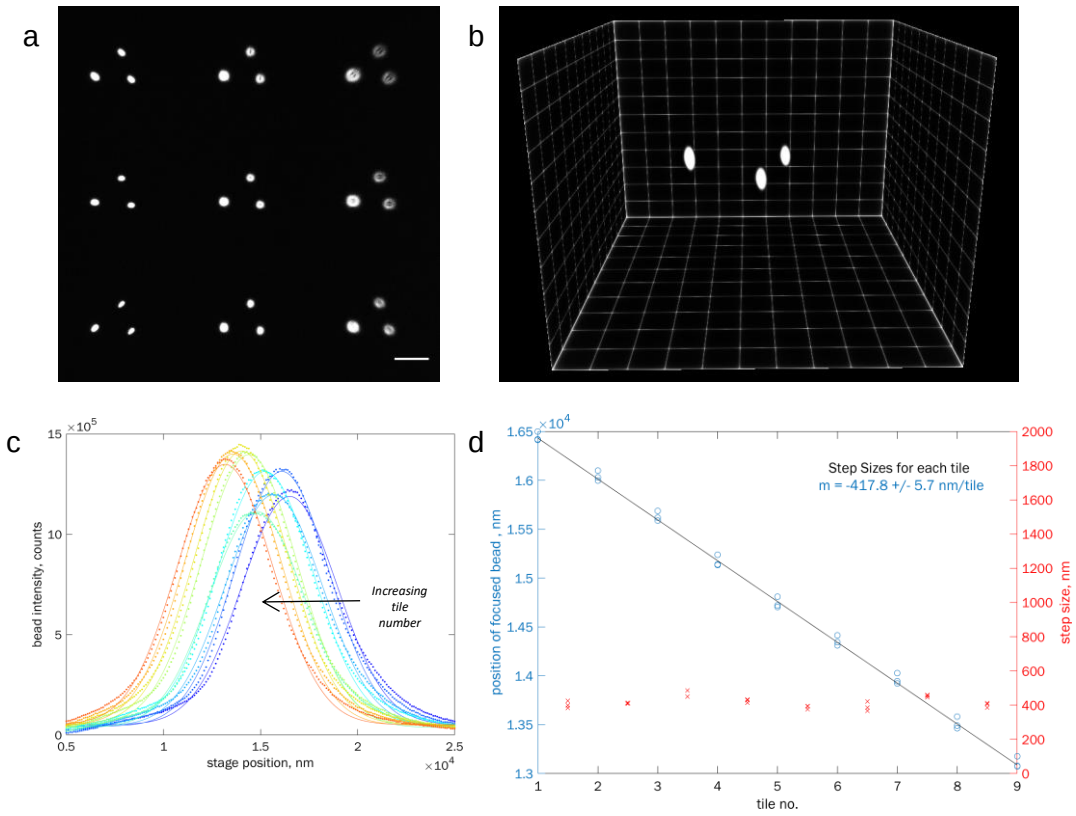

Figure S5**.** MFM characterization of a 400 nm focal-shift DOE from a z-stack of immobilized 200nm dia. red fluorescent beads. (a) MFM images of three 100nm red fluorescent beads immobilized to a coverslip. Beads are in-focus at the plane closest to the coverslip, i.e., the bottom left tile. Scale: 10 μm. (b) 3D reconstruction of beads after deconvolution. Grid: 3 μm/grid square. **(c)** Bead intensity as a function of stage position from the tile closest to the bottom coverslip and objective (1, blue) to the tile furthest from the coverslip (9, red). Gaussian fit (solid lines) for each intensity profile determines the z localization of the bead in each tile and therefore the position of the associated focal plane. **(d)** Analysis of Gaussian fitted intensity profiles from tile 1 to 9. The position of the focused bead is extracted from the mean (centroid) of the corresponding Gaussian fit (blue circles). The fitted slope (black line) is the average focal shift for each tile: 417.8 +/- 5.7 nm/tile (or per focal plane). The individual focal shifts (red crosses) are the difference of adjacent tile localizations. Note there are 3 values for each tile from the 3 beads in the image in (a).

The localization measurements of the 3 beads shown in Figure S5 was also used to determine the accuracy of the localization. The results of the z-axial positions (measured) vs. the true positions (from the z-axis piezo encoder) for 3 beads are shown in Figure S6. Figure S6a shows the results over the full range allowed by the MFM optical (9 planes with a 418nm focal shift between the planes) along with a line of slope = 1. As in Figure 2, there is a deviation from the line near the ends of the range that are a result of the increasingly poor determination of the bead locations due to the fact that the axial image of the bead is being increasingly

truncated as it approaches the first and last MFM focal planes. Therefore, the central range (~1.3um) shown in Figure S6b is used to determine the accuracy. The accuracy is determined as the standard deviation of the differences between the measured and true values of the axial location. The results for the 3 beads are combined and give 13nm for the accuracy over the 1.3um range.

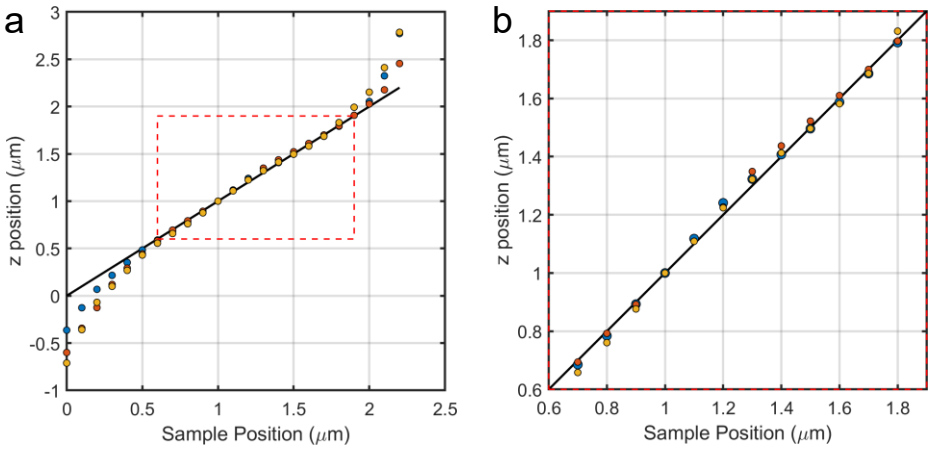

Figure S6. Accuracy determination for particle localization in MFM imaging and reconstruction for a 418nm focal shift DOE using Video 5 (a) The black line is the true position of the bead established with the piezo nano-positioner encoder. The colored points (blue, yellow, orange) are the measured positions after reconstruction and localization of the three beads. (b) The standard deviation is 13.1 +/- 0.2 nm in the 1.3 μm z range defined in the red box.

5. Measurement and 3D analysis of beads diffusing in solution.

As in the main text, we conducted measurements of 200nm dia. beads diffusing in 50% glycerol:water solutions. The expectation is for a uniform probability density function in the axial direction since the volume slab being sampled was ~30um from the bottom coverslip surface. Figure S7a shows an MFM image of the beads in the 9 tiles and video 6 show the imaging data. Figures S7b,c are a portion of the reconstructed 3D images of the beads in solution using the MTD-SEC-I approach (2 different renderings; the egg shapes in Figure S7c are a schematic creation in Imaris and not a reconstruction of the actual beads).

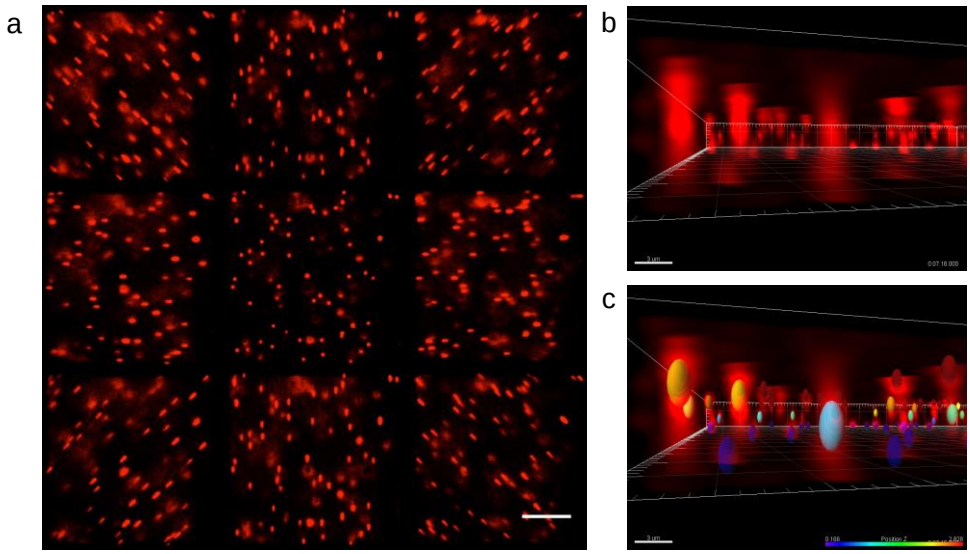

Figure S7. Measurement and particle localization for 200 nm diffusing beads in 50% glycerol solution. (a) Diffusing fluorescent beads measured at 20 Hz frame rate for 500 frames with 50 ms exposure time. Scale bar = 10 μm. (b) 3D reconstruction of beads using the MTD-SEC-I approach and final rendering and localization determination with Imaris. Each frame of the video data was preprocessed by deconvolution as described above in the SI. Scale bar = 3 μm. (c) 3D particle localization of reconstruction image. Ellipsoids are creations of the localization and the color coding shows the z position of each bead. White scale bars = 3 μm.

Figure S8a shows the distribution of log(counts) vs. z-position over the full range of the MFM optic. This is different than Figure 4b in the main text where the localizations near the limits of the axial range were omitted. The reason for that is clear from the U-shaped distribution in Figure S8b. The pile-up near the limits of the range results from the fact that the axial localization approach used here cannot have a centroid located beyond the 1st or 9th focal planes. This is clearly evident in video 7 of the 3D trajectories of the beads; the trajectories of the centroids do not extend beyond the upper and lower focal planes. The region between the 2 limits is rather flat and uniform as expected. Further corroboration of the fidelity of the reconstruction comes from an analysis of the dynamics. The transport of the beads is characterized by the 3D Ensemble Averaged Mean Square Displacement (EA-MSD) of their motion. The slope in the log(MSD) vs. log lag time plot is α=0.993, which is the expected results for Brownian diffusion (α =1).

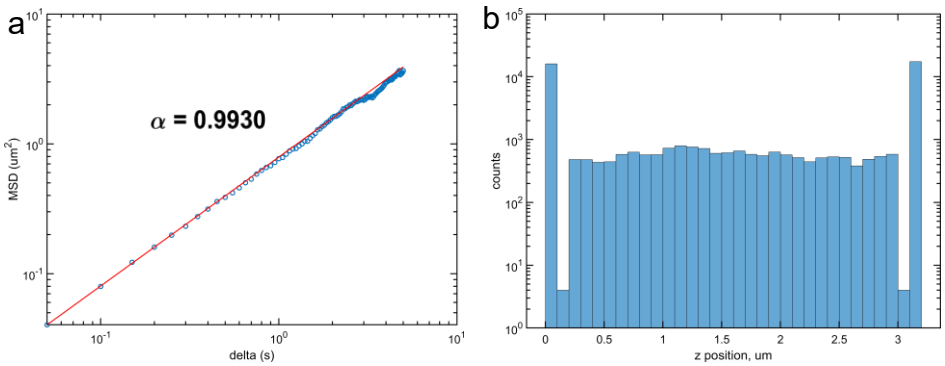

Figure S8**.** Dynamics and localization analysis of diffusing beads. (a) Ensemble-averaged MSD of diffusing beads from Figure S7. 19340 displacements averaged over 897 recorded trajectories. The slope of the log-linear fit (red line) $\alpha \approx 1$ is the diffusion scaling, which is signature of Brownian motion. (b) Histogram of the z position of each recorded localization. The distribution of the z localization is heavily biased to the extremes of the measurement range. These extremes were omitted from the MSD analysis as the axial motion is clearly distorted there.

Both Figure 4b and Figure S8b show some ripple structure (small deviations from a uniform distribution) that are greater than Poisson counting noise. The ripples also appear to be periodic. This might be associated with the precision of localization due to the Fisher information criterion, which gives more precision between the focal planes in MFM. We tested whether there is a non-uniform distribution of localizations by constructing a "meta-pixel" that can detect pixel locking error.[6,7] The analysis approach is schematically represented in Figure S9a and results of this analysis are shown in Figure S9b-c. The same data are represented in 2 ways. Figure S9b shows the localizations from all the bead data along a range of z that is equal to the 418nm focal shift (the data a collapsed onto a single such range to construct the meta-pixel) and spread out horizontally to allow visualization by shifting each localization horizontally by a random value chosen from a uniform distribution. The distribution of points looks uniform by eye. Figure S8b represents the meta-pixel data along z quantitatively by counts in bins. Again, the distribution is nearly uniform with some random noise. If the ripples observed in Figure 4b and Figure S7b where related to the Fisher information precision or some other periodic error, this would show up in the meta-pixel as a bias away from a uniform distribution.[6,7]

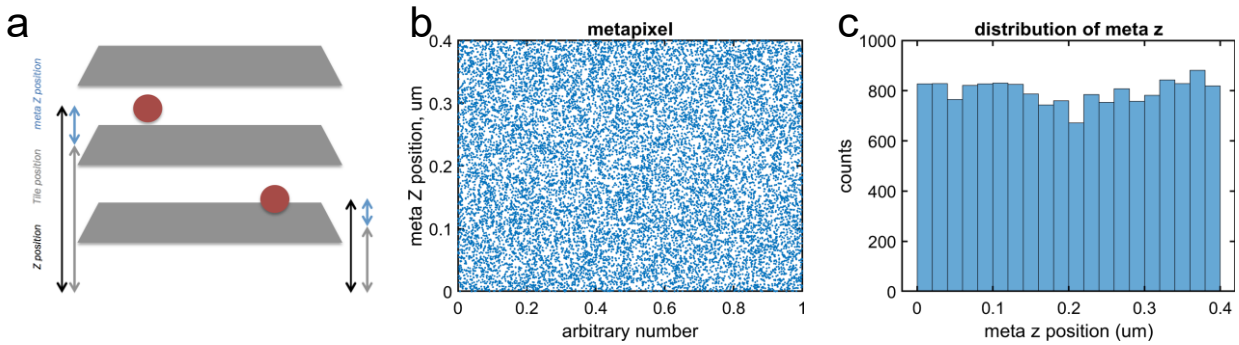

Figure S9. Analysis to ascertain localization bias from a possible pixel locking effect. (a) Schematic of 1D 'meta-pixel' calculation. The position in the meta-pixel (blue arrows) of the localized particle (red dots) is calculated as the difference between the actual z position (black arrows) and the nearest lower tile position (gray arrows). The gray tiles represent three focal planes measured by MFM. (b) 1D 'meta-pixel' construction from the z positions obtained from particle localization. The meta Z position, that is the position in the meta pixel, is mapped into 2D for visualization by assigning each meta z position a random number from a uniform distribution. We observe that meta-pixel mapping is random and uniform; visually there is no indication of 'pixel-locking'. (c) Histogram of meta Z positions. Distribution of the meta Z position is nearly uniform with a slight dip in probability near the center (~0.2nm) of the z axial meta-pixel.

Figure S10a shows a localization bias to the top and bottom of the analysis range as was noted in Figure S8. The cause for this was already discussed. The meta-pixel approach was repeated in segments to test localization bias in each analysis window. The meta-pixel analysis of 8 segments, i.e., each focal plane-to-focal plane interval, in Figure S10b shows a 'ripple' pattern of the z localization distribution. The dotted vertical lines are the locations of each MFM focal plane. The observed match between the small peaks in the distribution and the position of the focal plane suggests that the ripple structure occurs because there is a greater probability of localization at the focal planes.

This modulation of the axial localization probability is not consistent with the modulation of precision that is described by Fisher information theory. We believe the error arises from the image reconstruction approach, which we are investigating further. Nevertheless, the consistency of the results of 3D particle tracking by MFM with two DOEs designed with different focal lengths demonstrates that Nyquist sampling is not an issue the with particle tracking and localization approach that we have developed and report here.

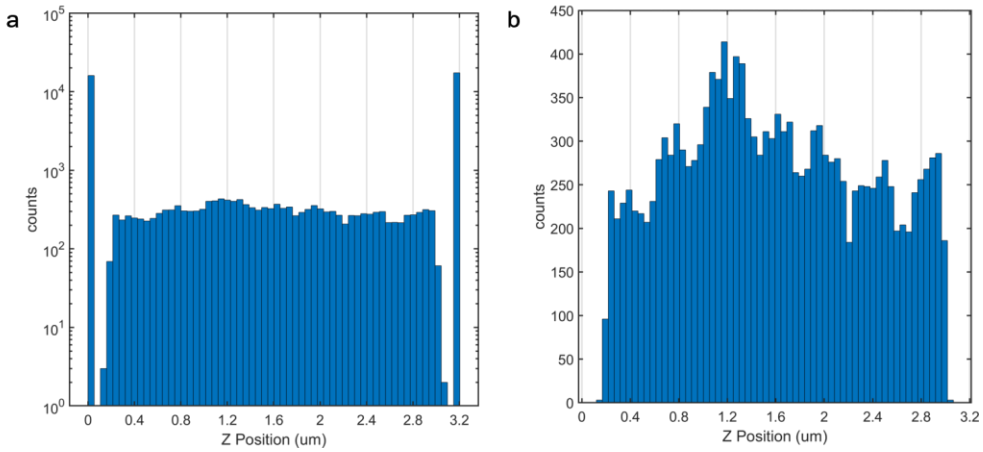

Figure S10. Meta-pixel analysis indicating periodic localization bias. (a) Log-linear plot of the full distribution of z information shown from Figure S8b with vertical lines denoting the location of the focal planes. (b) The same distribution omitting localizations that occur at the extremes of the axial range of the MFM. Vertical lines denote the locations of the MFM focal planes.

List of Supplementary Videos

Video 1: Sequence of MFM images (9 tiles) of 200nm dia. fluorescent beads diffusing in 1:1 glycerol:water solution ~50um above the bottom coverslip's top surface (20fps).

Video 2: MFM video of insulin-containing vesicles (granules) in live MIN6 cells (10fps). mCherry labelled granules in ~8 cells are tracked in the central part of the ~5.2um thick slab.

Video 3: Point spread function measurement of a 100nm dia. red fluorescent bead. The DOE optic used has a 650nm focal shift between adjacent tiles. Video z-stack is recorded in 50nm step sizes between frames.

Video 4: Point spread function measurement of a 100nm dia. red fluorescent bead. The DOE optic used has a 400nm focal shift between adjacent tiles. Video z-stack is recorded in 100nm step sizes between frames with 2sec exposure time for each frame.

Video 5: Three 200nm dia. red fluorescent beads using a 400nm focal shift DOE. Video z-stack is recorded in 100nm step sizes with 200nm exposure time. Measurement is used to characterize the DOE focal shift sizes between tiles and for shift correction for each tile.

Video 6: Time series video of 200nm dia. red fluorescent beads immersed in 50% glycerol in water solution. Video is recorded at 20Hz frame rate and plays at 2x speed.

Video 7: Trajectories of from freely diffusing beads shown in Video S3. Video plays at 10x speed.

References

1. Abrahamsson, S.; Chen, J. J.; Hajj, B.; Stallinga, S.; Katsov, A. Y.; Wisniewski, J.; Mizuguchi, G.; Soule, P.; Mueller, F.; Darzacq, C. D.; Darzacq, X.; Wu, C.; Bargmann, C. I.; Agard, D. A.; Dahan, M.; Gustafsson, M. G. L., *Nat. Methods* **2013,** 10, (1), 60-U80.
2. Wang, X.; Huang, X.; Gdor, I.; Daddysman, M.; Yi, H.; Selewa, A.; Haunold, T.; Hereld, M.; Scherer, N. F., *Proc. SPIE* **2018,** 10499, 104990R.
3. Toan, H.; Matthew, K. D.; Ying, B.; Alan, S.; Andrey, K.; Louis, H. P.; Norbert, F. S. *Rev. Sci. Instrum.* **2017,** 88, (5), 053702.
4. He, K.; Wang, Z.; Huang, X.; Wang, X.; Yoo, S.; Ruiz, P.; Gdor, I.; Selewa, A.; Ferrier, N. J.; Scherer, N.; Hereld, M.; Katsaggelos, A. K.; Cossairt, O., Computational multifocal microscopy. *Biomed Opt Express* **2018,** *9* (12), 6477-6496.
5. Pawley, J. A. *Handbook of Biological Confocal Microscopy **1995***
6. Yifat, Y.; Sule, N.; Lin, Y.; Scherer, N. F., *Sci. Reports* **2017**, 7, 16553.
7. Burov, S.; Figliozzi, P.; Lin, B.; Rice, L.; Scherer, N. F.; Dinner, A., *PNAS* **2016**, 114, (2), 221 - 226